

## Picosecond Absorption Spectroscopy of Excited States in BaBrCl with and without Eu Dopant and Au Codopant

Peiyun Li,<sup>1</sup> Sergii Gridin,<sup>1</sup> K. Burak Ucer,<sup>1</sup> Richard T. Williams,<sup>1,\*</sup> Mauro Del Ben,<sup>2</sup>  
Andrew Canning,<sup>2</sup> Federico Moretti,<sup>2</sup> and Edith Bourret<sup>2</sup>

<sup>1</sup>*Department of Physics, Wake Forest University, Winston Salem, North Carolina 27106, USA*

<sup>2</sup>*Lawrence Berkeley National Laboratory, Berkeley, California 94720, USA*



(Received 1 April 2019; revised manuscript received 11 June 2019; published 19 July 2019)

We perform picosecond absorption spectroscopy on BaBrCl samples that are undoped, doped with europium to make activated scintillators, and codoped with gold (as AuBr<sub>3</sub> in the melt) to increase light yield. The time-resolved measurements provide insights into the effects of interband excitation in BaBrCl, including identification of self-trapped-exciton absorption bands, the mechanism of energy transport from the host to the Eu activator, and the effects of Au codoping. First-principles electronic structure calculations of self-trapped-exciton relaxations in BaBrCl are presented. BaBrCl:Eu,Au is a beneficiary of two material modifications for improvement of performance that have been intensely investigated recently: a mixed-halide solid solution that is further modified by aliovalent codoping.

DOI: [10.1103/PhysRevApplied.12.014035](https://doi.org/10.1103/PhysRevApplied.12.014035)

### I. INTRODUCTION

Among scintillation materials for energy-resolved detection of ionizing radiation, two of the best-performing ones that have reached commercialization are LaBr<sub>3</sub>:Ce and SrI<sub>2</sub>:Eu. LaBr<sub>3</sub>:Ce with Sr codopant holds the current record for  $\gamma$ -energy resolution by a scintillator,  $\Delta E/E = 2.0\%$  at 662 keV [1]. SrI<sub>2</sub>:Eu probably holds the current record for light yield among commercialized scintillators, measured in the range of 90 000–120 000 photons/MeV [2–4]. While these are respective paradigms of two important technical performance criteria, both scintillators are expensive, both are very hygroscopic, and SrI<sub>2</sub>:Eu needs pulse-shape analysis to overcome a problem with self-absorption of the Eu scintillation light [5]. Cost and ruggedness are important concerns in most applications, and strategically so for security screening where widespread deployment is crucial. On several grounds, there remain reasons to continue searching for high-performance scintillators that are cheaper (e.g., due to ease of crystal growth) and are less hygroscopic.

In the same chemical family as SrI<sub>2</sub>:Eu but with even higher density and effective atomic number, BaI<sub>2</sub>:Eu has been investigated as a scintillator. However, it exhibits a light yield of only about 38 000 photons/MeV [6–8]. It was found that trading the pure iodide anions for a 50:50 halide mixture of Br and I in a barium mixed-halide salt yields decidedly better performance [9,10].

BaBrI:Eu scintillator crystals exhibit excellent light yield of 97 000 photons/MeV and energy resolution of 3.4% at 662 keV [10]. A number of barium mixed halides and mixed barium alkali iodides were also found to have good scintillation properties [11,12]. This may be part of the empirical trend noted by Gektin *et al.* [13] that mixed-ion crystals and solid solutions often exhibit better scintillation performance with regard to light yield and resolution than do the pure single-halide or single-cation versions. Even with its excellent scintillation characteristics, BaBrI:Eu is still hygroscopic and relatively difficult to grow to large size, so the search for good scintillators within the barium mixed-halide family continued, including demonstration of good performance and relative ease of crystal growth in BaBrCl:Eu [14]. Crack-free transparent crystals of BaBrCl can be grown, and the best-reported performance in BaBrCl doped with 5% Eu includes light yield of 55 000 photons/MeV and energy resolution of 3.55% at 662 keV in a small crystal [14].

At low temperature the crystal structure of BaBrCl is orthorhombic (space group *Pnma*) [15,16]. This is the same structure as that of BaCl<sub>2</sub>, BaBr<sub>2</sub>, and BaBrI, while BaBrF is tetragonal (space group *P4/nmm*). The relation between BaCl<sub>2</sub> and BaBr<sub>2</sub> and the mixed-halide structures is that BaCl<sub>2</sub> and BaBr<sub>2</sub> have two inequivalent halide sites, and so in the mixed halides the larger and smaller halide ions occupy different sites. This also means that in BaBrI, Br is the smaller halide ion and occupies a site different from the site it occupies in BaBrCl where it is the larger halide ion.

\*williams@wfu.edu

Some members of the general barium mixed-halide  $Ba(X,Y)$  family, especially  $Ba(F,Br):Eu$  are well known as storage phosphors for x-ray imaging [17–19]. The F center (halide vacancy trapping an electron) is found to play an essential role as a temporary electron trap (i.e., the storage step in the storage phosphor). The electron-binding energy of the F center in different members of the  $Ba(X,Y)$  family at room temperature controls whether the material functions as a storage phosphor or possibly as a scintillator [20].  $BaBrCl:Eu$  is one of the scintillators in this family, as noted above.

Our opening example of  $LaBr_3:Ce,Sr$  illustrates the remarkable success of aliovalent codoping in improving the already-excellent performance of  $LaBr_3:Ce$ . The success of  $LaBr_3:Ce,Sr$  helped promote widespread investigation of the effects of codoping on the performance of other scintillators [21–26]. Codoping is helpful in a number of scintillator materials, but particularly in halide scintillators the reasons are not always well understood and are likely not always the same. The present study deals with a finding by Shalapska *et al.* [27] that codoping of  $BaBrCl:Eu$  with trivalent Au produces a significant increase of light yield. It was shown that 0.1 mol %  $AuBr_3$  codoping in the melt tripled the scintillation light yield of  $BaBrCl$  doped with 0.5% Eu and caused a 40% increase in crystals doped with 5% Eu. At the same time, Au codoping diminished the slow component of scintillation decay, the so-called afterglow.

## II. EXPERIMENT

### A. Sample characteristics

The  $BaBrCl$  crystals are grown by the vertical Bridgman-Stockbarger method in vacuum-sealed quartz ampoules with use of high-purity (99.999%)  $BaBr_2$ ,  $BaCl_2$ ,  $EuBr_2$ , and  $AuBr_3$  from Sigma-Aldrich. Raw-material handling and crystal cutting and polishing are done in an Ar-filled glove box with  $H_2O$  and  $O_2$  concentration below 0.1 ppm. Before growth, the raw materials are dried in a vacuum at 120 °C overnight and the ampoule is subsequently sealed under a vacuum. The crystals are grown at 0.78 mm/h.

The crystals obtained are transparent, although the Au-(co)doped ones are characterized by the presence of a metallic gold layer on top of the boule [Fig. 1(a)], and the presence of molecular bromine is seen as an orange coloration of the ampoule [Fig. 1(b)], suggesting that  $AuBr_3$  is not stable under these growth conditions and it undergoes dissociation.  $Br_2$ , which is volatile at room temperature, fills the empty space in the ampoule and is clearly seen in the top part above the crystal. The color disappears quickly when the ampoule is opened, allowing the bromine gas to disperse in the dry box. For transient spectroscopy, the samples cut from the boules are polished and encapsulated in cells with fused-quartz windows while in a

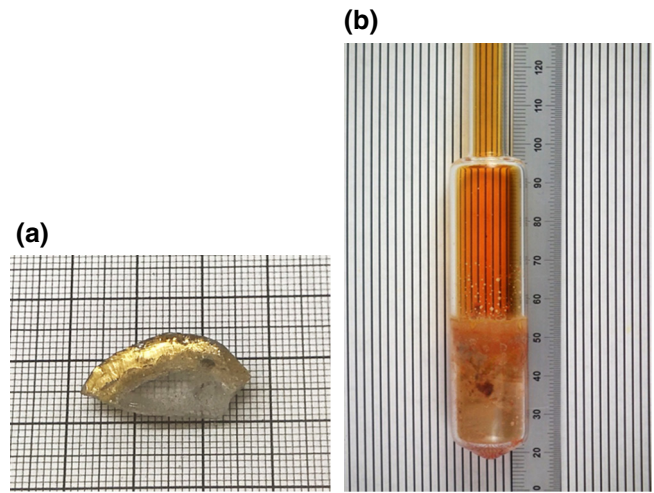


FIG. 1. (a) End portion of a  $BaBrCl:Eu$  crystal after being cut from the main portion of the grown boule. The piece is covered with a thin layer of metallic gold resulting from  $AuBr_3$  dissociation into elemental gold and bromine. (b) Photograph of the ampoule above the crystal grown from a  $BaBrCl:EuBr_3$  (0.1%) charge. In this photograph taken before opening of the ampoule after growth, the orange color is due to bromine gas ( $Br_2$ ). The smaller-diameter tube at top is used for ease of sealing.

nitrogen-filled glove box with less than 0.07 ppm  $O_2$  and less than 0.28 ppm  $H_2O$ . A list of the samples and their properties is given in Table I.

The impurity and Au content in representative  $BaBrCl$  as-grown crystals without and with doping is measured by glow-discharge mass spectrometry (GDMS). The main impurities detected are Na (a few parts per million by weight), I (170 ppm by weight), and Ca (a few parts per million by weight). Data obtained on O, C, and S are not reliable due to possible environmental contamination during sample preparation. GDMS on a melt-quenched  $BaBrCl:Eu$  sample codoped in the melt with 0.1%  $AuBr_3$  fails to find Au incorporated in the crystal above the detection limit of 0.9 ppm by weight. This null result is checked by extended-x-ray-absorption-fine-structure (EXAFS) spectroscopy on powdered single-crystal samples grown with Au in the melt, which also fails to find Au incorporated into the crystal.

TABLE I. Some properties of the  $BaBrCl$  samples studied in this work. Concentrations are given as mole percent in the melt and the ratio of Br to Cl is kept at 50/50 for all samples.

Crystal	Eu (mol %)	Au (mol %)	Thickness (mm)
$BaBrCl$ , undoped	0	0	2.05
$BaBrCl:Eu$	0	0.05	3.55
$BaBrCl:Eu$	0.5	0	2.3
$BaBrCl:Eu,Au$	0.5	0.1	2.2

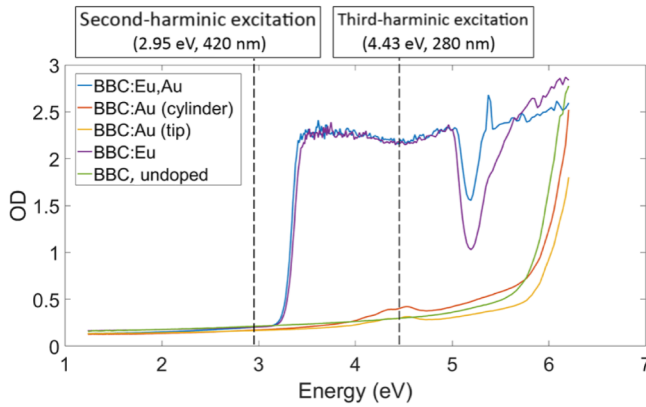


FIG. 2. Absorption spectra of the five samples studied before radiation, also indicating the second and third harmonics of the laser pulse. The third harmonic at 4.43 eV can generate electron-hole pairs of total energy 8.86 eV by two-photon absorption in undoped and Au-doped BaBrCl (BBC), and can produce resonantly enhanced multiphoton excitation as well as direct Eu excitation in Eu-doped samples.

### B. Measurement of picosecond absorption

The laser system and the main experimental method are described in Refs. [28,29]. The regeneratively amplified Ti:sapphire mode-locked laser delivers fundamental pulses at 10 Hz, 840 nm, and 200 fs. The band gap of BaBrCl has been reported to be approximately 7.3 eV [27]. Inspection of Fig. 2 along with knowledge of the band gap confirms that two-photon absorption of the 2.95-eV laser second-harmonic pulse would reach a final state only in the transparent “impurity edge” of BaBrCl, and so will not be useful for an interband pump pulse. The third-harmonic (280 nm, 4.43 eV) pump pulses with a duration of approximately 300 fs at the sample produce two-photon interband excitation of hot free carriers in the bulk BaBrCl crystal. The excess kinetic energy of the carrier pairs is  $8.86 - 7.3 = 1.56$  eV, offering a rough approximation of carrier energies in the phonon-mediated relaxation stage of  $\gamma$ -energy deposition. From Fig. 2, interband excitation of BaBrCl should be the main result of two-photon excitation by the third-harmonic laser pulses in both undoped and Au-doped BaBrCl. Two-photon absorption is confirmed by our measuring fluence-dependent transmission of the 4.43-eV pump beam, corresponding to the method in Ref. [30].

However, Fig. 2 shows that the Eu dopant present at 0.5 mol % in our Eu-doped and Eu,Au-codoped samples will strongly absorb the 4.43-eV pump pulses. Thus, we should view the experiments on all four sample doping types as comprising two possibly separate experiments: one in undoped and Au-doped samples probes absorption clearly induced by interband excitation of hot free carriers in the bulk crystal, and the other in Eu-doped and Eu,Au-codoped samples probes transient absorption induced by excitation involving one-photon absorption by

Eu, possibly as the first step of a resonantly enhanced multiphoton transition. One possibility for what may be measured in the experiments on Eu-doped samples is that the induced transient absorption spectra will characterize excited europium,  $\text{Eu}^*$ . We will call this “possibility (a).” Another possible outcome is that there will be resonantly enhanced production of free carriers. The third-harmonic pump-pulse energy in our experiment is  $20 \mu\text{J}$ , corresponding to pulse power of 70 MW and power density (irradiance) at the approximately-1-mm-radius pump spot of approximately  $2 \text{ GW}/\text{cm}^2$ . This power density deposits a significant fraction (approximately 50%) of the pump-pulse total energy in the 2-mm thickness of undoped BaBrCl by two-photon absorption. With Eu doping at such irradiance, it is likely that Eu will function as a resonant-enhancement intermediate state for two- and three-photon absorption producing mainly hot electrons and holes (i.e., most of the excited  $\text{Eu}^*$  produced should be photoionized by the same pulse). Whereas two-photon absorption is dominant via the virtual intermediate states in pure BaBrCl, resonant enhancement can make three-photon absorption dominant alongside two-photon absorption. We previously found indirect evidence of strong three-photon excitation resonantly enhanced by cerium in  $\text{LaBr}_3:\text{Ce}$ , in which the outcome was identified by picosecond spectroscopy to be electron-hole pairs relaxed in the form of self-trapped excitons [28]. The process can be approximately described as absorption of one photon to produce excited  $\text{Ce}^*$  or  $\text{Eu}^*$  as the case may be, followed by photoionization of the  $\text{Eu}^*$ -bound excited electron to the conduction band by a second photon, and charge transfer of an electron from the valence band into the  $\text{Eu}^*$  hole state using a third photon. At the end of this, Eu is left in its electronic ground state, some lattice vibration is generated, and there is a hot electron and hole sharing excess kinetic energy from the three photons absorbed. The resonantly enhanced three-photon absorption can produce electron-hole pairs with up to  $3 \times 4.43 = 13.29$  eV; that is, hotter than by two-photon absorption, which dominates in pure BaBrCl. We call resonantly enhanced two- and three-photon absorption “possibility (b)” that may be observed.

We can experimentally distinguish whether possibility (a) or possibility (b) is dominant in the actual measurements. The test is to observe and identify the initial induced absorption spectrum in the clear case of interband excitation of undoped and Au-doped BaBrCl samples, and then enquire whether the initial induced absorption spectrum in the Eu-doped samples is basically different from that or substantially the same as that in the samples without Eu.

The time resolution of induced absorption in undoped BaBrCl and Au-doped, Eu-doped, and Eu,Au-codoped BaBrCl was measured by the pump-probe picosecond absorption technique. By tuning the optical parametric amplifier (OPA) to a specific probe wavelength and varying the arrival time of the pump pulse, we plot the

delay time traces of induced transmission recorded by an amplified PbS detector in the spectral range from 1000 to 2900 nm. To cover the red-visible spectral range, the frequency of the infrared OPA output is doubled. The photodetector used in the spectral range from 575 to 1100 nm is a silicon detector. The total spectral range covered with the tunable OPA and its direct or frequency-doubled output ranges from 575 nm (2.16 eV) to 2800 nm (0.44 eV).

Each different wavelength measured is on a fresh spot of the sample. Before any pump exposure on a given spot, the probe-only transmitted signal ( $I_o$ ) is measured on the fresh spot, with 300 probe-only pulses averaged. This pristine  $I_o$  value is used as the reference signal to compute transient and residual induced absorption on the selected spot. The pump-induced change of the optical density (OD, also denoted  $D$ ) is calculated by the formula

$$\Delta D(t) = -\log_{10} \left( \frac{I(t)}{I_o} \right), \quad (1)$$

where  $I(t)$  is the transmitted signal at time  $t$  after the most-recent pump-pulse exposure. All experiments are conducted at room temperature.

### III. RESULTS

#### A. Stable $F_{Cl}$ and $F_{Br}$ absorption bands induced by electron-hole-pair generation in BaBrCl

Each sample is irradiated by the third-harmonic laser pulses (4.43-eV photons, two-photon absorption) at 10 Hz, averaging 30 shots for each of 100 delay settings comprising a pump-probe delay scan at a given wavelength. Thus, about 3000 pump pulses in 5 min exposure are accumulated in acquisition of a time-delay trace. To assess the residual color-center absorption produced, a spot on each sample is exposed to the pump pulses for 2 min at room temperature and then the sample is moved within about 3 min to a spectrophotometer for measurement of the optical absorption spectrum. In Fig. 3, the stable defect absorption measured in a Cary 50 UV-visible spectrophotometer after exposure to 1200 laser shots is compared for all four samples. Only the undoped BaBrCl sample exhibits stable absorption that can be recorded above the noise 3 min later in the spectrophotometer. This is supported by visual observation as recorded in the photograph inset. It shows a purple spot of color-center absorption that can be seen for several minutes up to 1 h after accumulated interband laser excitation (two-photon absorption—total 8.86 eV) at room temperature. It is visible to the eye only in the undoped sample. The offsets evident in the mostly flat spectra for the doped samples are probably due to differences in surface finish, including faint fogging of some of the encapsulated hygroscopic samples. A more-sensitive measurement by optically stimulated luminescence at room temperature reveals color-center bands at about 1.8 and 2.3 eV in the

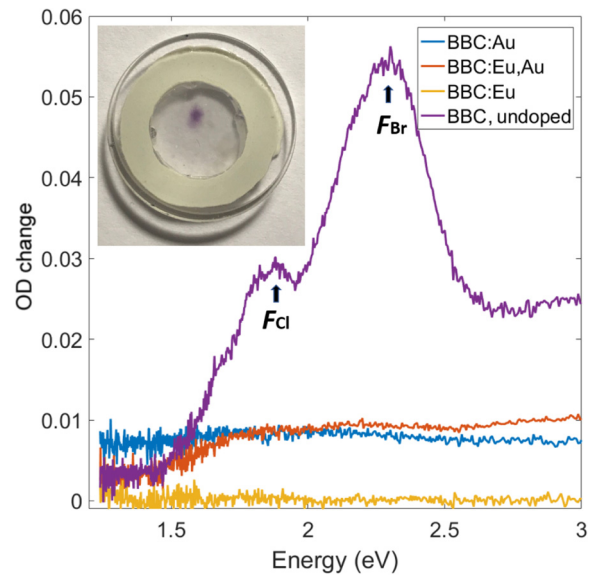


FIG. 3. Residual color-center spectra produced by exposure to 1200 shots of two-photon interband excitation at 10 Hz, measured by a spectrophotometer within approximately 3 min of the last shot for four samples with different doping conditions. The inset shows a photograph of the undoped BaBrCl (BBC) sample, showing purple color in the laser-irradiated spot.

Eu-doped sample as well as in the undoped sample but that are undetectable above baseline noise in the transmission spectrum shown in Fig. 3.

The most-prominent spectral features in Fig. 3 are the two absorption peaks at about 1.83 and 2.3 eV. These can be compared with peaks at 1.83 and 2.25 eV in published difference absorption spectra measured in BaBrCl:Eu by Meng *et al.* [31]. Difference absorption refers to the spectrum after X-ray exposure minus that before exposure. The 1.8-eV band was identified as due to  $F_{Cl}$  (F center on a chloride site) absorption and the 2.3 eV band was identified as due to  $F_{Br}$  (F center on bromide site) absorption by Bourret-Courchesne *et al.* [20] using density-functional theory calculations similar to those discussed in Sec. IV.

#### B. Time-resolved absorption measured with picosecond laser pulses in BaBrCl without and with dopants

Figure 4 shows time-resolved rise and decay curves of induced absorption at 700 nm (1.77 eV), which lies on the low-energy side of the absorption band of an F center on a Cl site ( $F_{Cl}$ ). The induced change in OD can be read from the vertical axis. Figure 4 displays data for each of the four different sample doping conditions. The absorption induced by a pump pulse is plotted for relative probe arrival times from  $t = -4$  ps to  $t = +16$  ps, where  $t = 0$  ps corresponds to coincident arrival of the pump and probe pulses. The meaning of negative delay is that the probe

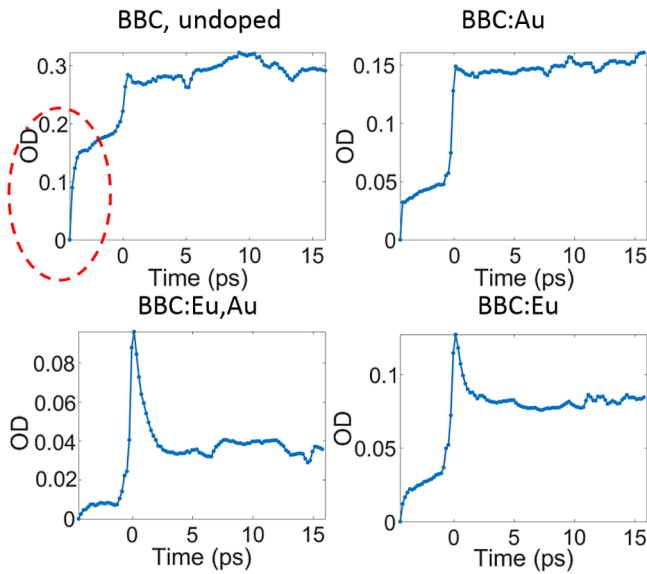


FIG. 4. Time dependence of induced absorption in BaBrCl (BBC) samples that are (clockwise from upper left) undoped, Au doped (in the melt), Eu doped, and Eu,Au codoped (in the melt). These measurements are at a wavelength of 700 nm (1.77 eV), which is within the  $F_{Cl}$  band. The circled feature registered at negative delay in the undoped sample is the “pedestal” of induced residual absorption, effectively versus accumulated laser shot number as discussed in the text.

pulse arrives before the pump pulse it is paired with, and so the probe pulse probes the effect of the pump pulse in the proceeding pair 0.1 s earlier, as well as residual absorption from still earlier pulses at 10 Hz. Each plot represents 100 time-delay values spanning the stated time range, and at each time delay, the signal from 30 pump-probe pulse pairs is averaged.

We look first at the negative-delay feature circled on the undoped-BaBrCl response in Fig. 4, which we call the “pedestal” of residual absorption. The pedestal rises with a very steep slope at first and then this changes to a much lower slope as the delay time approaches  $t = 0$ . Although the horizontal axis is labeled “Time (ps),” it really represents accumulated pump-pulse shots received at 10 Hz in the negative-delay region. Thus, the pedestal plot registers purely the buildup of induced absorption versus radiation dose measured in units of accumulated pump pulses. This may seem like using an ultrafast sledgehammer to do a nearly-steady-state 100-ms radiation-damage experiment, but in fact it is important and useful to see this stage of radiation response registered quantitatively on the same plot as the picosecond transient absorption measured at positive delay. The steep rise and subsequent saturation of residual F-center absorption in the pedestal region is a phenomenon well known from the alkali-halide literature. The steep initial rise versus dose is often referred to as the “easy stage of F-center formation,” in which ionizing

radiation produces free electrons that are captured on pre-existing halide vacancies. The shape of the pedestal that we observe closely resembles the growth of the F band under x-ray radiation for alkali-halide crystals measured by Rabin and Klick [32]. Saturation occurs when the pre-existing vacancies in the probed volume have all captured electrons. That saturation is followed by the harder, “second stage” of F-center production in which one actually creates new vacancy-interstitial pairs (F center and H center pairs), with the residual 100-ms survivors having a shallow slope versus dose.

The easy formation of F centers by electron capture on pre-existing vacancies might impact scintillation performance (e.g., by removing electrons from the recombination pool that could otherwise contribute to light emission). A quick conclusion that appears just from inspection of the negative-delay region in Fig. 4 is that the pedestal of easy F-center formation by populating old vacancies is largest in the undoped sample, next largest in the Au-doped sample, but smaller in the Eu-doped sample, and smallest of all in the Eu,Au-codoped sample. The stable (approximately 3 min) F centers are formed appreciably in only undoped BaBrCl, and not observable in any of the doped samples. In contrast, the 100-ms surviving F centers contributing to the pedestal in Fig. 4 can be observed in all samples, with the amount of suppression depending on the amount of doping.

Next we consider the positive-delay portion of the data in Fig. 4. When the probe pulse is at a positive delay relative to the pump pulse, it measures the change in transmittance produced by the associated pump pulse that arrived just a few picoseconds earlier, as typically understood in pump-probe experiments. This produces the big vertical jump at  $t = 0$  ps delay for all four samples shown. The picosecond pump-induced signal rides on top of the pedestal, which therefore serves as a “recent baseline” for all positive delays.

From the plots for the undoped and Au-doped samples in the top row in Fig. 4, the response at positive delay is similar for both samples. It is a sharp step up from the saturated pedestal, rising from 10% to 90% in about 300 fs. This corresponds to the duration of the amplified pump pulse, implying a very fast rise of induced absorption. The rise is followed in the undoped and Au-doped samples by an initial fast decay with an amplitude of less than 10% followed by flat or slightly rising absorption out to 16 ps. The height of the fast rise up from the pedestal at  $t = 0$  ps is approximately equal ( $\Delta D \approx 0.1$ ) for both the undoped sample and the Au-doped sample. From these data, the effect of the Au doping seems mainly to be a suppression of the “easy-F-center” pedestal from  $\Delta D \approx 0.18$  in the undoped sample to  $\Delta D \approx 0.048$  in the Au-doped sample. The simplest way to achieve this would be by putting AuBr<sub>3</sub> in the melt if this suppresses bare halide-ion vacancies, including Cl<sup>-</sup> vacancies, which are singled out simply because we are looking at the  $F_{Cl}$  wavelength in Fig. 4.

Now we look at plots for the Eu-doped and Eu,Au-codoped samples in the bottom row in Fig. 4. The size of the fast rise above the pedestal level at  $t = 0$  ps is still about the same,  $\Delta D \approx 0.1$ , as in the undoped and Au-doped samples. Most noticeable is that in both samples containing Eu there is a very rapid decay (approximately 1 ps) from the maximum induced absorption just after  $t = 0$  ps. The rapid rise and decay appears as a spike of absorption at  $t \geq 0$  ps. Since Fig. 4 shows absorption in the region of the  $F_{Cl}$  band, one might try to interpret the fast spike of absorption just after the pump pulse in the two samples containing Eu as additional absorption from some Eu charge state produced on top of normal F centers. However, the “on top of” supposition does not work because the 10-ps plateau with Eu present is much lower than the 10-ps plateau absorption of F centers in both of the non-Eu-doped crystals in Fig. 4. Supposition of an induced Eu charge state in competition with F-center production does not make much sense either, because the supposed Eu-state absorption drops by up to 70% in about 2 ps. One would be losing too many Eu excited states to be consistent with the good light yield of this material, which for 5% Eu doping achieves 55 000 photons/MeV or almost 100% of the theoretical maximum light yield based on estimation of invested energy  $2.5E_{\text{gap}}$  per electron-hole pair with  $E_{\text{gap}} \approx 7.3$  eV. We temporarily refer to the fast-decaying spikes in Fig. 4 as “Eu attacking the induced 700-nm absorption,” and then try to assign the absorption and the attack mechanism after considering the spectrum of induced transient absorption.

The effect of the dopants on the induced absorption at 700 nm if attributed to  $F_{Cl}$ -like defects can be summarized in four observations:

(a) The undoped BaBrCl exhibits the largest pedestal of residual  $F_{Cl}$ -like-defect absorption. A prompt further rise of  $F_{Cl}$ -center absorption at  $t = 0$  ps (pump-probe coincidence) occurs on top of the pedestal of accumulated residual absorption. This steep rise at  $t = 0$  ps represents new F-H defect pairs created together from the perfect lattice. On the picosecond timescale of Fig. 4, one cannot tell if they persist, but they are mostly transient on the basis of the slope of the pedestal’s hard stage. Since 30 shots are averaged at each increase of 0.2 ps in delay time, we divide the absorption accumulated during the “hard stage” of the pedestal in undoped BaBrCl,  $\Delta D \approx 0.04$ , by the approximately 480 accumulated shots composing that part of the pedestal. Then the induced residual F-band  $\Delta D$  in the hard stage is roughly  $10^{-4}$  per shot in undoped BaBrCl. Compare this with the vertical rise of induced transient F-band absorption that is seen in Fig. 4 to be  $\Delta D \approx 0.1$  per single shot. This is reminiscent of results from transient absorption spectroscopy in alkali halides, particularly KCl and KBr [33].

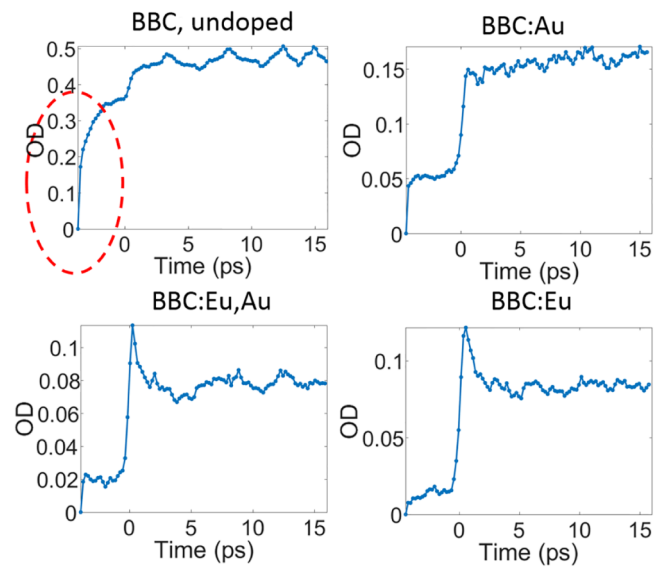


FIG. 5. Time dependence of induced absorption measured at 575 nm (2.16 eV),  $F_{Br}$ -band region. BBC, BaBrCl.

(b) Doping with Au in the melt suppresses the pedestal of easy F centers to about 30% of its undoped value, but seems to do little else. In particular, Au does not “attack” the 700-nm absorption the way that Eu does.

(c) Doping with Eu suppresses the pedestal of easy F centers to about 20% of the undoped pedestal value, and it quickly “attacks” the fresh 700-nm absorption induced by the pump pulse.

(d) Codoping with Eu and Au has a similar effect on 700-nm absorption as doping with Eu. The easy-F-center pedestal is suppressed to about 5% of the undoped pedestal and the attack on the 700-nm-induced  $F_{Cl}$ -center absorption appears to be the most complete with codoping (i.e., reduction to about 32% of the maximum above the pedestal background within 2 ps).

The above measurements and analysis are repeated for other wavelengths across the spectral range accessible to our OPA and frequency-doubled-OPA, from 2800 nm (photon energy 0.44 eV) to 575 nm (photon energy 2.16 eV). The characteristic time profiles introduced in Fig. 4 occur and change in a fairly systematic way versus probed photon energy. Figure 5 presents data for 575 nm (2.16 eV), which is spectrally on the low-energy side of the  $F_{Br}$ -defect band.

The same general discussion as above for the induced 700-nm absorption versus doping applies to the 575-nm absorption (2.16 eV) in the  $F_{Br}$ -band region. The pedestal of easy residual F-center formation by electron capture on old vacancies is even higher in this  $F_{Br}$  region, consistent with the relative heights of stable  $F_{Br}$  and  $F_{Cl}$  defects measured by the spectrophotometer in Fig. 4. For both F-center wavelengths, when either Au or Eu is added, the

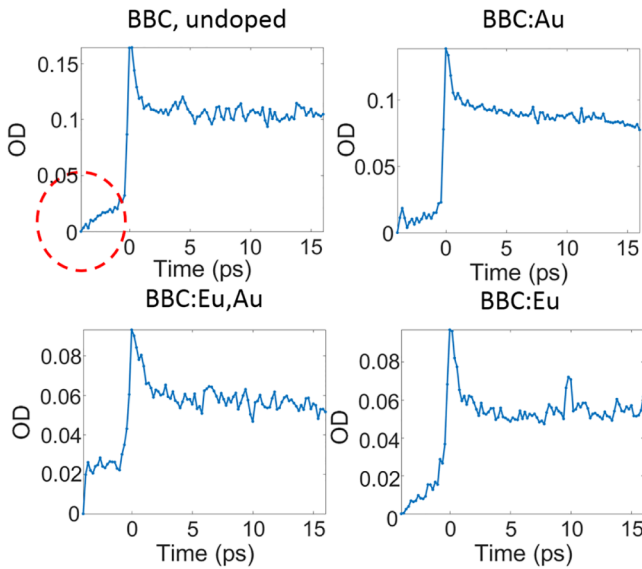


FIG. 6. Time dependence of induced absorption measured at 1200 nm (1.03 eV). BBC, BaBrCl.

negative-delay pedestal of “easy” F-center formation is reduced.

The attack by Eu on the 575-nm absorption associated with  $F_{Br}$  is not as strong as it is on 700-nm absorption associated with  $F_{Cl}$ . Whereas Au codopant seems to assist the attack of Eu on the  $F_{Cl}$  absorption at 700 nm (Fig. 4), Au does not obviously assist the attack of Eu on the  $F_{Br}$  absorption at 575 nm (Fig. 5).

Figure 6 shows time profiles at a probe wavelength of 1200 nm (photon energy 1.03 eV), which is out of the spectral range of either the  $F_{Cl}$ -defect band or the  $F_{Br}$ -defect band. Yet it exhibits significant transient absorption induced by interband excitation. The entire rise and decay traces for this wavelength appear almost identical regardless of doping, suggesting that the band at 1200 nm is a universal property of the BaBrCl host; 1200 nm is the peak of a transient induced absorption band that we suggest is due to a type-II self-trapped-exciton (STE), using terminology from alkali halides. The “attack” of induced absorption at 1200 nm cannot be attributed to Eu in this case. It is more general, independent of dopant type or doping at all. We suggest it could be nonlinear quenching of the type-II STE at densities on the order of  $10^{18} \text{ cm}^{-3}$  needed to record reasonable optical absorption in this experiment.

### C. Transient absorption spectra: defect bands and STE

Next we show spectral plots constructed from time-dependent absorption data at multiple wavelengths. Figure 7 plots the induced absorption spectra for the maximum absorption occurring in  $0 \text{ ps} < t < 1 \text{ ps}$  as black

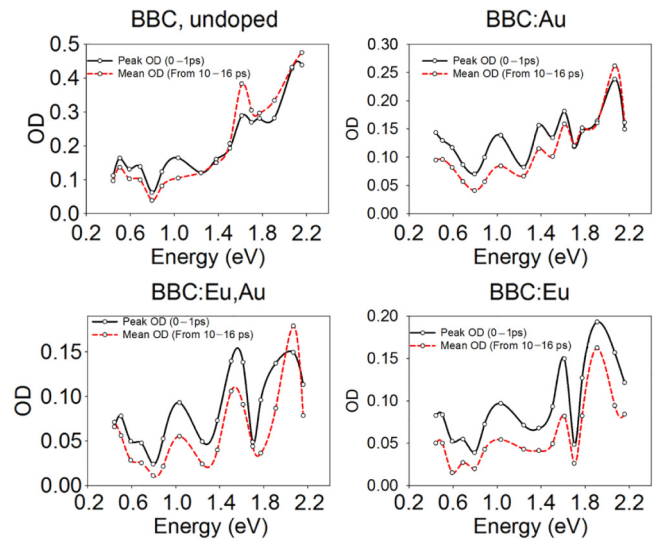


FIG. 7. Induced absorption spectra for the  $0 \text{ ps} < t < 1 \text{ ps}$  peak (black lines), and the  $10 \text{ ps} < t < 16 \text{ ps}$  plateau (dashed red lines), for each of the BaBrCl (BBC) doping choices labeled.

lines, and the plateau value of absorption averaged from 10 to 16 ps as dashed red lines, for each of the four doping conditions. The spectral density of the measurement points is relatively sparse because of the need to use a fresh spot of the sample for each wavelength. Even so, one can recognize a commonality of four induced absorption bands that seem to be shared by all the samples despite different doping choices. The time-dependence traces discussed earlier point to distinct differences in rise and/or decay characteristics versus doping. In contrast, the spectra point more to similarities in spectral shape common to all samples without much regard to doping. This suggests that the main four spectral bands are characteristic of BaBrCl itself rather than of particular dopants.

To highlight the features independent of doping and increase the signal-to-noise ratio, Fig. 8 shows averages of the induced spectra for all three samples without Eu (i.e., undoped, Au doped from the tip of the boule, and Au doped from the cylinder part of the boule) plotted in black, and spectra for samples with Eu (i.e., Eu only, Eu,Au codoped) plotted in red. Figures 8(a) and 8(b) show spectra of the peak OD ( $0 \text{ ps} < t < 1 \text{ ps}$ ) and of the OD persisting in the plateau averaged from 10 to 16 ps, respectively. In Figs. 8(a) and 8(b), induced absorption at the peak and plateau is measured relative to the pristine-sample reference  $I_0$  as described in Eq. (1), so the plotted OD spectrum includes the “pedestal” of residual F-center absorption induced by all previous shots.

Figures 8(c) and 8(d) show the difference spectra, “peak minus plateau” and “peak minus pedestal.” Both of these difference spectra exclude the pedestal of residual F centers. In Fig. 8(d), the general rise toward high photon energy associated with the pedestal is eliminated, and

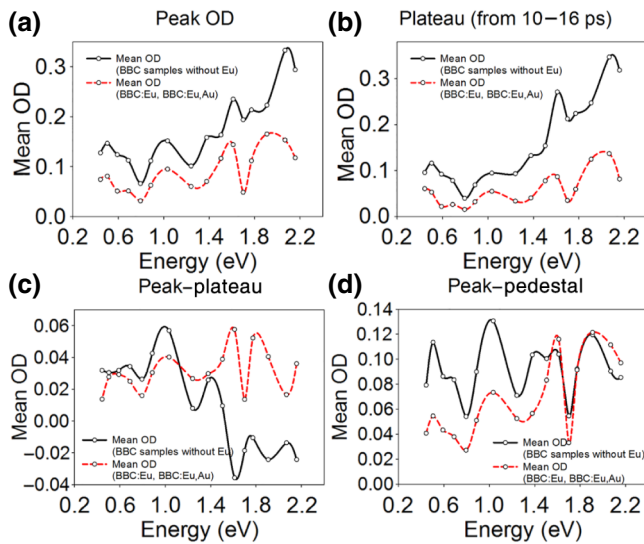


FIG. 8. Induced absorption spectra averaged for all BaBrCl (BBC) samples without Eu doping (black lines) and for all BaBrCl samples with Eu doping (dashed red lines) for the maximum absorption achieved in  $0 \text{ ps} < t < 1 \text{ ps}$  in (a) and the averaged absorption in the plateau defined as  $10 \text{ ps} < t < 16 \text{ ps}$  in (b). Difference spectra are presented in (c),(d). With terms defined in the main text, the difference spectra are peak minus plateau and peak minus pedestal.

the four induced absorption bands common to all sample dopings are revealed as having comparable strength at approximately 1.9, 1.6, 1.0, and 0.5 eV. Figure 8(c) confirms our observation that the peak-plateau difference, earlier called “attack on induced F-band absorption by Eu dopant,” is confined mainly to the bands at approximately 2.0 and 1.6 eV. The list of the four absorption-band peaks just given does not include the two F-band peaks at 1.83

and 2.3 eV known from stable spectra. The picosecond total absorption spectra for both the peak (less than 1 ps) and the plateau (approximately 10 ps) features have “F-like” bands at approximately 2.0 and 1.6 eV, in each case about 0.2 eV lower than the known stable  $F_{Br}$  and  $F_{Cl}$  peaks.

Although Fig. 7 is suggestive of four peaks common to spectra of all of the differently doped samples, the spectral resolution in each data set is poor due to the sparse points, and so we examine whether the suggested peaks are significant relative to variance in multiple measurements taken on different sampled spots at each wavelength. We have data in the same spectral series on a total of five different samples: undoped, Au doped from the tip of the boule, Au doped from the cylinder part of the boule, Eu doped, and Eu,Au codoped. To examine if there are spectral peaks characteristic of the host BaBrCl rather than the dopants, we average data for all five samples and compute the standard deviation at each wavelength, shown as error bars representing one standard deviation above and below the average in Fig. 9(a). In addition to display of the error bars, the five separate measurements are shown as circles identified by color with respective sample dopings. The average value at each wavelength is shown as a triangle, and the triangles are connected by straight-line segments as a guide for the eye. The variance represents not only statistical noise but also differences from doping and location on the crystal boule or sample surface. In any case it represents an upper limit of the noise among the five samples. The quantity plotted is the “peak-minus-pedestal” normalized OD. The difference plot eliminates the pedestal of residual F-center absorption, which changes continually during a multishot measurement especially in the undoped sample and is not the transient induced signal of interest.

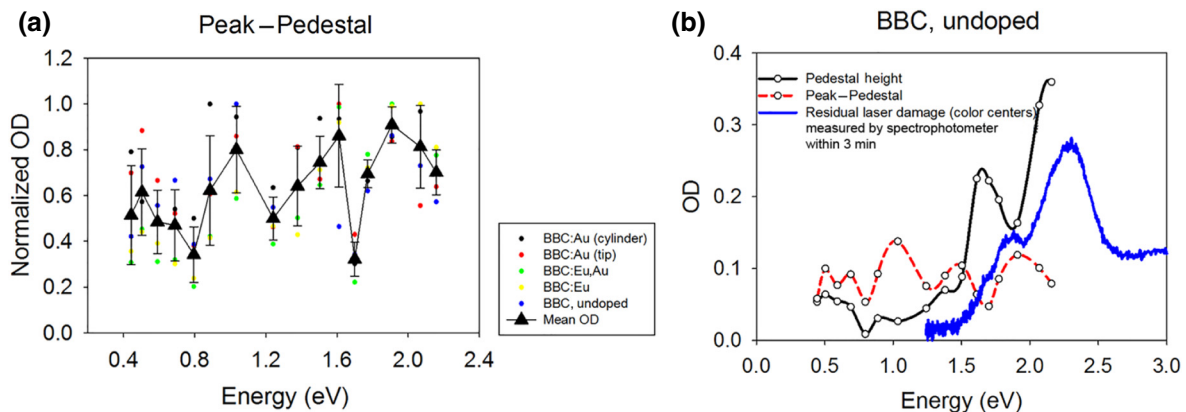


FIG. 9. (a) Transient induced absorption (peak minus pedestal) for five different samples normalized at the maximum optical density of each spectrum shown by small circles (color coded in the legend). Their mean value at each wavelength is shown by triangles, with bars representing one standard deviation above and below the mean. The mean values are connected by straight-line segments. (b) Spectra of stable F-band absorption after approximately 3 min (noisy, blue curve), pedestal height due to saturated residual F centers measured after at least 100 ms (black curve), and the difference curve, peak minus pedestal, due to F centers newly created within 1 ps after the pump pulse (dashed red curve) in undoped BaBrCl (BBC).

The spectra for different samples are normalized at their maximum OD before averaging.

The four peaks in Fig. 9(a) exceed the standard deviation at each respective peak by factors of 11, 3.8, 3.8, and 3.3 from high energy to low energy. The peak-to-adjacent-valley difference divided by the mean peak-and-valley standard deviation gives ratios of 6.9, 3.6, 2.0, and 1.2 in the same order. These ratios support the conclusion that the peaks are real relative to noise and furthermore that the surviving peaks characterize properties of the host BaBrCl rather than particular properties of the dopants.

In Fig. 9(b), the dashed red spectrum, black spectrum, and noisy, blue spectrum represent absorption characteristic of about 1 ps, 100 ms, and 3 min after the latest pump pulse that generated electron-hole pairs. There are three F-band-like pairs of absorption peaks in Fig. 9(b), each shifted spectrally from the others. The noisy, blue spectrum shows the stable  $F_{\text{Br}}$  and  $F_{\text{Cl}}$  absorption bands with peaks at 2.3 and 1.83 eV. The black spectrum is that of metastable F-like centers registered in the pedestal, formed as little as 100 ms after electron-hole-pair generation. Recall from the discussion in Sec. III B that the pedestal is measured at negative probe-pump delay, where the probe measures effects of the pump pulse in the previous pulse pair 100 ms earlier, along with residual effects of prior pulse pairs. The pedestal spectrum is shifted about 0.2 eV to the low-energy side of the stable peaks. By analogy to alkali-halide studies [33], these could be F centers perturbed by proximity to interstitial H centers created at the same time. These metastable perturbed F centers must exist for up to 100 ms to be observed as residual. The dashed red spectrum (peak minus pedestal) in Fig. 9(b) has a large, approximately-0.4-eV shift to the low-energy side of the stable F bands (i.e., peaks at 1.95 and 1.5 eV), and may be regarded as due to highly perturbed F centers in a close F-center-H-center pair. It was shown first in alkali-halide studies that a nearest-neighbor F-H vacancy-interstitial pair has significant overlap of the F-center electron with the H-center hole and thus behaves as a lattice-relaxed electronic excited state of the crystal, an off-center self-trapped exciton [34]. In preparation for further discussion of relaxed electronic excited states in BaBrCl and as background for some use of analogies and nomenclature from the alkali halides, we present in the following section electronic structure calculations of self-trapped excitons and defects in BaBrCl.

#### IV. ELECTRONIC STRUCTURE CALCULATIONS OF SELF-TRAPPED EXCITONS AND DEFECTS

We perform first-principles electronic structure calculations as a guide for interpreting observations on transient absorption induced by electron-hole-pair production in BaBrCl. Many detailed experimental studies using specialized techniques have been used to construct what is now

a reasonably complete understanding of STEs and their conversion to F-H defect pairs in alkali halides, including optically detected electron paramagnetic resonance [35], electron-nuclear double resonance [36], polarized spectroscopy with oriented self-trapped holes and self-trapped excitons [37], time-resolved absorption [38], and experiments conducted on mixed crystals [39], and under applied stress [40]. While STE phenomena have continued to be discovered in additional materials through to the present day, no other materials have received the attention of so many experimental techniques focused on their STE properties as alkali halides, except possibly  $\text{SiO}_2$  due to its technological importance. Instead, recent electronic structure calculations with demonstrated ability to capture the features of exciton and hole self-trapping offer an economical tool often used to explore relaxed excited states, polarons, and defect formation in newly considered materials. We summarize here the results of electronic structure calculations on self-trapped excitons and some relevant defect properties in BaBrCl. Similarities of structure and properties to self-trapped excitons in alkali halides are also pointed out.

We perform first-principles electronic structure calculations with VIENNA AB INITIO SIMULATION PACKAGE (VASP) [41,42] and CP2K [43,44]. VASP was used for bulk-band-structure and defect-level calculations using the Perdew-Burke-Ernzerhof (PBE) generalized-gradient-approximation functional, while CP2K was used for PBE0-hybrid-functional calculations for the  $V_k$  center and STE calculations. CP2K has the advantage with its mixed basis Gaussian and plane waves that it has a very efficient implementation of hybrid functionals, allowing us to easily simulate systems of hundreds of atoms required to accurately model the atomic relaxation of the  $V_k$  center and corresponding STE states. The generalized-gradient-approximation functional does not correctly model the  $V_k$  center, and more-advanced methods, such as hybrid functionals, are required. More-detailed explanations of these calculations along with more-extensive results will be the subject of a future publication.

The first calculations we perform use VASP for band-structure calculations of BaBrCl and BaBrCl with Br and Cl vacancies. We use cell sizes of 192 atoms and the projector-augmented-wave approach with the PBE functional and pseudopotentials. The halide-vacancy calculations are performed by our removing one halide from the supercell and relaxing the atomic positions, with the cell size fixed at the bulk structure, until the forces on each atom are below 0.01 eV/Å. The vacancy states have a hydrogenlike character modified by the lattice structure, so the Cl-vacancy state is a distorted  $1s$  state. The depth of the Cl-vacancy state below the conduction-band minimum is 0.45 eV, while the Br-vacancy state is 0.4 eV below the conduction-band minimum. By purely energetic arguments, the Cl-vacancy state would then be a

stronger electron trap than the Br-vacancy state and more likely to form. In relation to the absorption experiments described in Sec. III C we also look at the excited states of the halide-vacancy F centers. As mentioned earlier, the excited states of the F center tend to be hydrogenlike, and like the  $1s$ -character ground state are very localized. We can therefore scan up through the empty states above the Fermi level to find the excited states associated with the F centers. The first excited state has a distorted  $2s$ -type character. We then calculate the energy difference between the empty first excited state and the  $1s$  ground state to have some measure of the absorption energy of the two different F centers. While this is a very approximate way to calculate the absorption energy of the F centers, it gives some measure of the ordering of the absorption energies of the two F centers. We find that the difference in energy between the excited state and the ground state of the Cl and Br F centers is 1.8 and 2.1 eV, respectively, in remarkably good agreement with the experimental results of 1.83 and 2.25 eV and helping us to identify which absorption is associated with which halide F center. This also places the excited states of the two F centers in the conduction band.

The next step in our calculations is to look at the formation of  $V_k$  centers and corresponding STEs using a constrained-occupancy approach with hybrid functionals using CP2K. To perform these calculations, we again take a large supercell based on the bulk structure, and then move two halide atoms closer together and remove an electron to form a self-trapped hole. Atomic relaxation is then done on the cell to obtain the equilibrated  $V_k$ -center geometry. To model an STE we constrain the system to be in the excited triplet state by blocking the number of electrons in one of the spin channels to be larger than that in the other spin channel, this time performing the calculation on a neutral cell. As previously mentioned, there are typically three types of STE relaxations in halide materials [34]. For alkali halides, type I has a geometry close to the  $V_k$ -center geometry where two halide atoms move symmetrically together and the hole and electron states are centered on the two halide atoms. In type II, one halide moves closer to the neighboring halide, which remains at the bulk lattice site. In type III, a halogen atom moves through to a neighboring unit cell, creating an interstitial atom and leaving a vacancy (Frenkel-type defect). Type III can be thought of as an F-center–H-center pair. In the case of the binary alkali halides, the crystal structures are primarily face-centered cubic and some body-centered cubic, so there is only one unique geometry of a halide pair for forming the three types of STEs. In the case of BaBrCl, since it has two types of halides and an orthorhombic crystal structure, the situation is more complicated. There are seven possible halide-pair geometries for this crystal structure, consisting of Cl–Cl, Cl–Br, and Br–Br pairs. If they can all form type-I, type-II, and type-III STEs, then there are 21 different possible STE geometries. We do not perform

an exhaustive study of the stability of all possible STE geometries in BaBrCl, but examples of the stablest type-I, type-II, and type-III geometries we find are shown in Figure 10. From a theoretical point of view we find that these types of STEs are stable in a similar way to the alkali halides and LaBr<sub>3</sub>. We also investigate the migration of these types of STEs as well as properties of hole and electron traps. We perform these calculations of the exciton states by molecular-dynamics simulations at high temperature to determine migration pathways and then use the nudged-elastic-band method to determine the migration-energy barriers. While we find the migration pathways can be rather complex on moving between the different types of stable STEs, the energy barriers to migration are typically on the order of 0.1 eV. Thus, the STEs are mobile at room temperature and can easily migrate to the activator. The timescale for the STE to move to a neighboring site is on the order of picoseconds at room temperature. We also study the migration of H-center hole traps associated with interstitial halides that can be formed by  $\gamma$  rays through creation of F-center–H-center pairs. Again we find the energy barriers for migration of H centers to be on the order of 0.1 eV. More details of these calculations will be presented in a future publication.

## V. DISCUSSION

### A. Self-trapped excitons and other transient defects in BaBrCl

Our measurements of excitation-induced transient absorption spectra in undoped BaBrCl as well as doped BaBrCl (Figs. 7–9) reveal four main spectral bands, at about 0.5, 1.0, 1.6, and 1.9 eV. The first-principles electronic structure calculations presented in this work reveal that many of the STE relaxed-excited-state characteristics now familiar from alkali halides and alkaline-earth halides are also predicted for the alkaline-earth mixed halide crystal BaBrCl. This includes finding relaxed configurations of STEs similar in some regards to those previously labeled in alkali halides as type I, type II, and type III (on-center  $V_k$ -like, moderately-off-center incomplete F-H pair, and strongly-off-center nearest-neighbor F-H pair). With the expectation thus supported for finding STE spectra in BaBrCl that seem to follow patterns established in the alkali halides and alkaline-earth halides, we suggest that the 0.5-eV band in BaBrCl is due to a type-I STE. The 1-eV band is proposed to be due to a type-II STE, and the 1.6- and 1.9-eV transient bands are attributed to type-III STEs involving partially formed chloride-ion and bromide-ion vacancies, respectively. The hybrid-functional density-functional theory calculations used in this study cannot predict the STE excited-state transition energies, but predict the relaxed STE configurations that underpin the qualitative optical transition assignments suggested above.

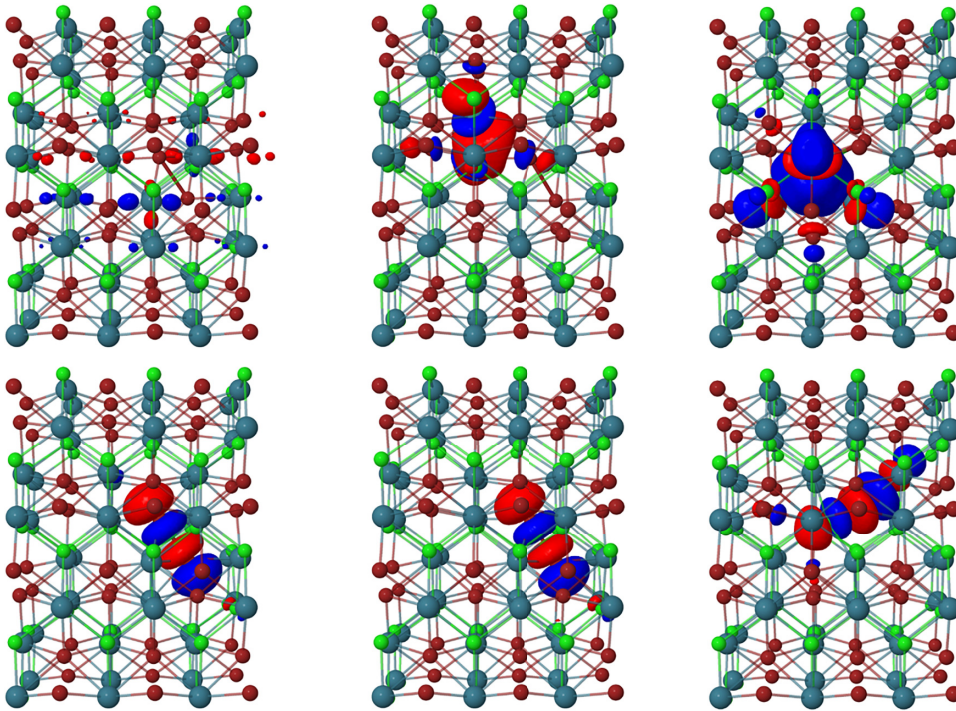


FIG. 10. Charge-density isosurfaces: from left to right, type I, type-II, and type-III STEs in BaBrCl. Electron states are shown at the top and hole states are shown at the bottom.

The absorption signatures of these relaxed STE states appear in undoped BaBrCl within the laser pulse width of 300 fs, and that seems to be the extent of excited states that can be detected within the 0.45–2.16-eV spectral range probed in our experiment, aside from the pedestal of residual F-band absorption discussed previously. In terms of spectral bands of transient optical absorption produced, the doped samples seem to behave similarly to the undoped sample. Thus, on the basis of observations within our spectral range, it appears that on the timescale of 1 ps, the main form of deposited energy from multiphoton non-resonant or resonant interband absorption is self-trapped excitons.

### B. Energy Transfer from STEs to Eu in BaBrCl:Eu

On the basis of the experimental result that the initial pulse-induced absorption bands in Eu-doped samples are similar to the bands already identified as due to STEs in undoped BaBrCl, we conclude that interband electron-hole-pair excitation and subsequent rapid relaxation to STE relaxed states is the common starting point in our experiment, whether Eu is present or not. When present, Eu acts as a resonant intermediate state for multiphoton interband excitation at the 2 GW/cm<sup>2</sup> pump irradiance used. One of the reasons for undertaking the present study of picosecond transient absorption was to seek information on the mechanism of energy transfer from electron-hole pairs in the BaBrCl host to the Eu dopant ions.

As previously noted, we do not observe a direct signature of Eu\* excited states in the transient absorption

spectrum from 0.45 to 2.16 eV. In studies of LaBr<sub>3</sub>:Ce by a similar technique, we found an induced-absorption signature of Ce\* attributed to photoionization of the excited electron to the conduction band at an energy of 2.1 eV. Because the band gap of BaBrCl is wider than that of LaBr<sub>3</sub> (7.3 eV vs 5.9 eV), it may be that the similar photoionization transition exceeds the 2.16-eV limit of our OPA probe. A distinct effect that is observed in our spectroscopy is the rapid “attack” on induced absorption in the type-III-STE bands (1.6 and 1.9 eV) when Eu is present, and only then. We suggest that this rapid loss of STE population in the presence of Eu is due to energy transfer from STEs to Eu, since the 40% loss in the STE population would otherwise contradict the light yield of BaBrCl:Eu, which is near the theoretical maximum if  $\beta E_{\text{gap}} = 2.5E_{\text{gap}}$ . We cannot rule out that some Eu\* may also be produced by the laser pulse since Eu\* absorption seems invisible in our spectral range. However, we also observe that the strength of induced STE absorption at  $t \approx 0$  ps in BaBrCl doped with 0.5% Eu is about the same ( $\Delta D \approx 0.1$ ) as in undoped BaBrCl. This implies that most of the interband excitations result in STE even in Eu-doped crystals, and that energy transfer from STEs to Eu\* should be regarded as the main route to populating Eu\* in BaBrCl:Eu.

Given the observed approximately 1 ps for the “Eu attack” attributed to energy transfer from STEs to Eu\*, dipole-dipole transfer at nearest-neighbor distance seems the likely mechanism. In LaBr<sub>3</sub>:Ce, the 1-ps dipole-dipole transfer time was encountered only when the excitation pulse involved resonant excitation by Ce dopant so that the electron-hole pairs were produced adjacent to Ce [28].

When a laser harmonic that avoided resonant absorption of Ce was used, the transfer time was observed on the slower timescale of 69 ps for 4.4% Ce doping, attributed to dipole-dipole transfer averaged over a spread of distances falling within the  $R_{dd}$  transfer range, which is typically on the order of 3 nm. As discussed in Sec. II, we do not have the experimental option of avoiding Eu-resonant interband excitation in BaBrCl:Eu, and thus observe only the transfer from the STE to nearest-neighbor Eu. The transfer time is about 1 ps.

Dexter [45] calculated a dipole-dipole transfer time of 1-ps at nearest-neighbor separation in NaCl under the assumption of good overlap of the emission and absorption spectra. The dipole-dipole transfer rate is proportional to the overlap of donor emission and acceptor absorption spectra. In BaBrCl, the STE emission band identified by Shalapska *et al.* is broad and centered at approximately 5 eV. The Eu absorption spectrum of BaBrCl:Eu in Fig. 2 extends up to 5 eV and thus overlaps the low-energy side of the STE emission band. Our transient absorption spectra show that the effect of “Eu attack” (being attributed to dipole-dipole transfer) is significant only for the two type-III-STE bands at about 1.6 and 1.9 eV, not for the type-I-STE and type-II-STE bands. In alkali halides, the highly relaxed type-III STEs always have the largest Stokes shift of luminescence among the possible STE configurations [34]. Attributing the low-energy (4.5–5 eV) luminescence to type-III STEs in BaBrCl, we may suppose that type-I-STE and type-II-STE luminescence occurs at still higher energy (5–6 eV), out of resonance with Eu absorption. Pushing this interpretation of the STE spectrum in Ref. [27] beyond what the authors intended, we note that it appears as a three-component luminescence band, and only the low-energy component has good overlap with the Eu absorption spectrum.

## VI. CONCLUSIONS

Our data indicate that Au doping does not make a noticeable difference in any of the picosecond time-resolved experiments, except in affecting the size of the pedestal of residual F-band absorption. It suppresses the pedestal of residual F centers, implying that it reduces the concentration of pre-existing halide vacancies that can capture electrons to form “easy-stage” residual F centers composing the pedestal. A likely effect of bare-halide-vacancy concentration on scintillation would be as a competitor for the electron in radiation-produced electron-hole pairs that could otherwise contribute to light emission. If one or both of the  $F_{Cl}$  and  $F_{Br}$  centers formed from pre-existing vacancies hold on to trapped electrons for significantly longer than the  $Eu^*$  lifetime, there would be a shift of scintillation decay time toward long-tail emission or afterglow. Such components that exceed the

shaping time are not counted in pulse-height analyzers. A plausible hypothesis for the beneficial effects of Au codoping to both increase light yield and decrease slow decay is that Au suppresses the concentration of pre-existing halide vacancies, thus decreasing the drain on prompt electron-hole recombinations. This conclusion is similar to that reached by Shalapska *et al.* [27] based on measurements of light yield and afterglow fraction.

Our experiments show that Eu doping is even more effective than Au doping in suppressing the residual F-center pedestal. Furthermore, taking into account both Figs. 4 and 5, we conclude that Au codoping in Eu-doped crystals does not consistently suppress the pedestal more than Eu doping alone. Can these observations still be consistent with the basic hypothesis suggested above that Au suppresses the competing halide-vacancy electron traps even in Eu-doped crystals? We postulate that the effect of Au added in the melt is to suppress halide-ion vacancies. While Eu (0.5%) is observed to be even more effective than Au (0.1%) at suppressing the pedestal, we do not assume that isovalent  $Eu^{2+}$  operates in the same way as aliovalent  $Au^{3+}$  to affect the residual F-center pedestal. In the literature on storage phosphors, an F center close to a hole captured on or complexed with a Eu ion may contribute its electron by tunneling or thermal release to combine with a hole associated with Eu, resulting in the  $Eu^*$  luminescent state.

The essential point is that tunneling recombination of F and Eu close pairs gives suppression of the residual F-center pedestal that depends on Eu concentration. This suppression mechanism by Eu doping does not imply that the isovalent  $Eu^{2+}$  suppresses the concentration of halide-ion vacancies. *That is*,  $Eu^{2+}$  and  $Au^{3+}$  can separately achieve F-center pedestal suppression by different and independent actions. In this hypothesis, the  $Eu^{2+}$  suppression mechanism acts on the longevity of the F centers after they have formed, whereas the  $Au^{3+}$  suppression mechanism prevents the formation of the “easy F centers” in the first place by eliminating pre-existing halide vacancies that can trap electrons.

Shalapska *et al.* concluded “that the addition of Au in this material leads to a lower probability of charge carrier trapping at defect sites.” The stated conclusion of Shalapska *et al.* left it open as to “whether the lower trapping probability is related to a general reduction in the concentration of defects or to a modification of the electron/hole migration and transfer processes in favor of charge carrier recombination on the luminescent centers.” Our time-resolved data and the mechanism suggested above support the first part, that Au doping results in a general reduction in the concentration of halide-ion vacancies. Furthermore, conclusions from our time-resolved experiments specify that the second possibility in the two-part conclusion of Shalapska *et al.* is linked directly to the first. Removing

halide vacancies and their effect in breaking up electron-hole pairs created by ionizing radiation suppresses the slow STH migration and tunneling transfer processes to the benefit of rapid STE formation followed by picosecond-scale dipole-dipole transfer to Eu.

There is a related issue of what happens to the holes in undoped BaBrCl to allow metastability of the residual F centers in the face of possible F-H recombination. For guidance on this, we can go to the alkali-halide literature on F and H centers at various temperatures. The H centers are known to be very mobile at room temperature and considerably below, so they are moving rapidly. It was shown that the H centers clump into larger aggregates of multiple H centers, from di-H centers (labeled  $V_4$  centers) [46] up to larger clusters [47] and dislocation loops [48]. These are relatively stable at room temperature and soak up a lot of H centers in specific aggregates, which therefore are trapped at considerable distance from F centers, which remain more uniformly distributed.

The hypothesis we describe supposes that Au doping prevents in some way most of the pre-existing halide vacancies that could support easy F-center production. For this action, Au does not actually have to be present in the crystal at the time of picosecond spectroscopy and/or scintillation! It may have exerted its effect chemically in the melt. This is important because GDMS and EXAFS measurements indicate that very little Au is incorporated from the melt into the sample. Then how can Au doping exert control over pre-existing halide-ion vacancies?

A likely mechanism is that introduction of AuBr<sub>3</sub> in the growth ampoule enriches the melt in Br<sup>-</sup> anions relative to stoichiometric BaBrCl, suppressing anion vacancies [27]. Another possibility is scavenging of impurities by Au<sup>3+</sup> in the melt. Monovalent-alkali-ion impurities substituting for Ba<sup>2+</sup> in BaBrCl would appear negative because of the Madelung potential on the site occupied and could be charge compensated by halide vacancies. Since Au<sup>3+</sup> on a Ba<sup>2+</sup> site appears positive, it may associate in the melt with effectively negative substitutional alkali cations or substitutional divalent carbonate anions in BaBrCl, for example. Segregation of Au at the growth interface could eliminate the impurity pair. We have not yet determined which of the possible AuBr<sub>3</sub>-related mechanisms is responsible for the halide-vacancy suppression that our absorption measurements indicate.

### ACKNOWLEDGMENTS

This work was supported by the U.S. Department of Energy, National Nuclear Security Administration, Office of Defense Nuclear Nonproliferation (LB15-ML-GammaDetMater-PD3Jf) under Contract No. AC02-05CH11231. The portion carried out at Wake Forest University was under subcontract from Lawrence Berkeley National Laboratory.

- [1] M. S. Alekhin, J. T. M. De Haas, I. V. Khodyuk, K. W. Krämer, P. R. Menge, V. Ouspenski, and P. Dorenbos, Improvement of  $\gamma$ -ray energy resolution of LaBr<sub>3</sub>:Ce<sup>3+</sup> scintillation detectors by Sr<sup>2+</sup> and Ca<sup>2+</sup> co-doping, *Appl. Phys. Lett.* **102**, 161915 (2013).
- [2] E. V. van Loef, C. M. Wilson, N. J. Cherepy, G. Hull, S. A. Payne, W. Choong, W. W. Moses, and K. S. Shah, Crystal growth and scintillation properties of strontium iodide scintillators, *IEEE Trans. Nucl. Sci.* **56**, 869 (2009).
- [3] N. Cherepy, S. A. Payne, S. Asztalos, G. Hull, J. Kuntz, T. Niedermayr, S. Pimputkar, J. Roberts, R. D. Sanner, T. M. Tillotson, E. van Loef, C. M. Wilson, K. S. Shah, U. N. Roy, R. Hawrami, A. Burger, L. Boatner, W. Choong, and W. W. Moses, Scintillators with potential to supersede lanthanum bromide, *IEEE Trans. Nucl. Sci.* **56**, 873 (2009).
- [4] E. Rowe, P. Bhattacharya, E. Tupitsyn, M. Groza, A. Burger, N. J. Cherepy, S. A. Payne, B. W. Sturm, and C. Pédrini, A new lanthanide activator for iodide based scintillators: Yb<sup>2+</sup>, *IEEE Trans. Nucl. Sci.* **60**, 1057 (2013).
- [5] P. Beck, N. Cherepy, S. A. Payne, E. L. Swanberg, K. E. Nelson, P. A. Thelin, S. E. Fisher, S. Hunter, B. Wihl, K. S. Shah, R. Hawrami, A. Burger, L. Boatner, M. Momayezi, K. T. Stevens, M. Randles, and D. Solodovnikov, Strontium iodide instrument development for gamma spectroscopy and radioisotope identification, *Proc. SPIE Int. Soc. Opt. Eng.* **9213**, 92130N (2014).
- [6] G. Gundiah, G. Bizarri, S. M. Hanrahan, M. J. Weber, E. D. Bourret-Courchesne, and S. E. Derenzo, Structure and scintillation of Eu<sup>2+</sup>-activated solid solutions in the BaBr<sub>2</sub>-BaI<sub>2</sub> system, *Nucl. Instr. Methods Phys. Res., A* **652**, 234 (2011).
- [7] Z. Yan, G. Gundiah, G. A. Bizarri, E. C. Samulon, S. E. Derenzo, and E. D. Bourret-Courchesne, Eu<sup>2+</sup>-activated BaCl<sub>2</sub>, BaBr<sub>2</sub> and BaI<sub>2</sub> scintillators revisited, *Nucl. Instrum. Methods Phys. Res. Sect. A: Accel., Spectrom., Detectors Assoc. Equip.* **735**, 83 (2014).
- [8] N. J. Cherepy, G. Hull, A. D. Drobshoff, S. A. Payne, E. van Loef, C. M. Wilson, K. S. Shah, U. N. Roy, A. Burger, L. A. Boatner, W. Choong, and W. W. Moses, Strontium and barium iodide high light yield scintillators, *Appl. Phys. Lett.* **92**, 083508 (2008).
- [9] E. D. Bourret-Courchesne, G. Bizarri, S. M. Hanrahan, G. Gundiah, Z. Yan, and S. E. Derenzo, BaBrI:Eu<sup>2+</sup>, a new bright scintillator, *Nucl. Instrum. Methods Phys. Res. Sect. A: Accel., Spectrom., Detectors Assoc. Equip.* **613**, 95 (2010).
- [10] G. Bizarri, E. D. Bourret-Courchesne, Z. Yan, and S. E. Derenzo, Scintillation and optical properties of BaBrI:Eu<sup>2+</sup> and CsBa<sub>2</sub>I<sub>5</sub>:Eu<sup>2+</sup>, *IEEE Trans. Nucl. Sci.* **58**, 3403 (2011).
- [11] E. D. Bourret-Courchesne, G. A. Bizarri, R. Borade, G. Gundiah, E. C. Samulon, Z. Yan, and S. E. Derenzo, Crystal growth and characterization of alkali-earth halide scintillators, *J. Cryst. Growth.* **352**, 78 (2012).
- [12] E. D. Bourret-Courchesne, G. Bizarri, R. Borade, Z. Yan, S. M. Hanrahan, G. Gundiah, A. Chaudhry, A. Canning, and S. E. Derenzo, Eu<sup>2+</sup>-doped Ba<sub>2</sub>CsI<sub>5</sub>, a new high-performance scintillator, *Nucl. Instrum. Methods Phys. Res. Sect. A: Accel., Spectrom., Detectors Assoc. Equip.* **612**, 138 (2009).

- [13] A. V. Gektin, A. N. Belsky, and A. N. Vasil'ev, Scintillation efficiency improvement by mixed crystal use, *IEEE. Trans. Nucl. Sci.* **61**, 262 (2014).
- [14] Z. Yan, T. Shalapska, and E. D. Bourret, Czochralski growth of the mixed halides BaBrCl and BaBrCl:Eu, *J. Cryst. Growth.* **435**, 42 (2016).
- [15] Inorganic Crystal Structure Database (ICSD), collection code 35458.
- [16] S. A. Hodorowicz, E. K. Hodorowicz, and H. A. Eick, Preparation and characterization of the system BaBr<sub>x</sub>Cl<sub>2-x</sub>: The structure of BaBrCl, *J. Sol. State Chem.* **48**, 351 (1983).
- [17] M. Sonoda, M. Takano, J. Miyahara, and H. Kato, Computed radiography utilizing scanning laser stimulated luminescence, *Radiology* **148**, 833 (1983).
- [18] S. Schweizer, Physics and current understanding of X-ray storage phosphors, *Phys. Status Solidi Appl. Res.* **187**, 335 (2001).
- [19] S. Schweizer, J. M. Spaeth, and T. J. Bastow, Generation of F centres and hole centres in the nonstoichiometric X-ray storage phosphor BaFBr, *J. Physics: Condens. Matter* **10**, 9111 (1998).
- [20] E. D. Bourret-Courchesne, G. A. Bizarri, and A. Canning, Role of impurities and defects in determining the scintillation properties of mixed halide materials, (2016), report of Project LB15-V-GammaDetMater-PD3Jf, Advanced Materials for Detectors, unpublished.
- [21] K. Yang, P. R. Menge, J. J. Buzniak, and V. Ouspenski, in *2012 IEEE Nuclear Science Symposium and Medical Imaging Conference Record (NSS/MIC)* (IEEE, 2012), p. 308.
- [22] P. Guss, M. E. Foster, B. M. Wong, F. P. Doty, K. Shah, M. R. Squillante, U. Shirwadkar, R. Hawrami, J. Tower, and D. Yuan, Results for aliovalent doping of CeBr<sub>3</sub> with Ca<sup>2+</sup>, *J. Appl. Phys.* **115**, 34908 (2014).
- [23] F. G. A. Quarati, M. S. Alekhin, K. W. Krämer, and P. Dorenbos, Co-doping of CeBr<sub>3</sub> scintillator detectors for energy resolution enhancement, *Nucl. Instrum. Methods Phys. Res. Sect. A: Accel., Spectrom., Detectors Assoc. Equip.* **735**, 655 (2014).
- [24] N. Shiran, A. Gektin, Y. Boyarintseva, S. Vasyukov, A. Boyarintsev, V. Pedash, S. Tkachenko, O. Zelenskaya, and D. Zosim, Modification of NaI crystal scintillation properties by Eu-doping, *Opt. Mater. (Amst)* **32**, 1345 (2010).
- [25] K. Yang and P. R. Menge, Improving  $\gamma$ -ray energy resolution, non-proportionality, and decay time of NaI:Tl<sup>+</sup> with Sr<sup>2+</sup> and Ca<sup>2+</sup> co-doping, *J. Appl. Phys.* **118**, 213106 (2015).
- [26] I. V. Khodyuk, S. A. Messina, T. J. Hayden, E. D. Bourret, and G. A. Bizarri, Optimization of scintillation performance via a combinatorial multi-element co-doping strategy: Application to NaI:Tl, *J. Appl. Phys.* **118**, 84901 (2015).
- [27] T. Shalapska, F. Moretti, E. Bourret, and G. Bizarri, Effect of Au codoping on the scintillation properties of BaBrCl:Eu single crystals, *J. Lumin.* **202**, 497 (2018).
- [28] P. Li, S. Gridin, K. B. Ucer, R. T. Williams, and P. R. Menge, Picosecond absorption spectroscopy of self-trapped excitons and transient Ce states in LaBr<sub>3</sub> and LaBr<sub>3</sub>:Ce, *Phys. Rev. B* **97**, 144303 (2018).
- [29] K. B. Ucer, G. Bizarri, A. Burger, A. Gektin, L. Trefilova, and R. T. Williams, Electron thermalization and trapping rates in pure and doped alkali and alkaline-earth iodide crystals studied by picosecond optical absorption, *Phys. Rev. B* **89**, 165112 (2014).
- [30] P. Liu, W. L. Smith, H. Lotem, J. H. Bechtel, N. Bloembergen, and R. S. Adhav, Absolute two-photon absorption coefficients at 355 and 266 nm, *Phys. Rev. B* **17**, 4620 (1978).
- [31] X. Meng, Y. Wang, H. Jin, and L. Sun, BaBrCl:Eu<sup>2+</sup>: A new promising X-ray storage phosphor, *J. Rare Earths* **24**, 503 (2006).
- [32] H. Rabin and C. Klick, Formation of F centers at low and room temperatures, *Phys. Rev.* **117**, 1005 (1960).
- [33] R. T. Williams, M. N. Kabler, W. Hayes, and J. P. Stott, Time-resolved spectroscopy of self-trapped excitons in fluorite crystals, *Phys. Rev. B* **14**, 725 (1976).
- [34] K. S. Song and R. T. Williams, *Self-trapped excitons*, Springer Series in Solid-State Sciences Vol. 105 (Springer-Verlag, Berlin, Heidelberg, 1993).
- [35] M. J. Marrone, F. W. Patten, and M. N. Kabler, EPR in Triplet States of the Self-trapped Exciton, *Phys. Rev. Lett.* **31**, 467 (1973).
- [36] A. Wasielea, D. Block, and Y. Merle d'Aubigne, ENDOR of the self-trapped exciton in KCl, *J. Phys. C* **11**, 4201 (1978).
- [37] M. N. Kabler, Low-temperature recombination luminescence in alkali halide crystals, *Phys. Rev.* **136**, A1296 (1964).
- [38] R. T. Williams and M. N. Kabler, Excited-state absorption spectroscopy of self-trapped excitons in alkali halides, *Phys. Rev. B* **9**, 1897 (1974).
- [39] K. Kan'no, K. Tanaka, and T. Hayashi, New aspects of intrinsic luminescence in alkali halides, *At. Proces. Induced Electron. Excitation Non-Metallic Solids*, 253 (1990).
- [40] M. Itoh, S. Hashimoto, and N. Ohno, Self-trapped exciton luminescence in dilated NaI crystals—relaxation process of excitons in alkali halides—, *J. Phys. Soc. Jpn.* **60**, 4357 (1991).
- [41] G. Kresse and J. Furthmüller, Efficient iterative schemes for ab initio total-energy calculations using a plane-wave basis set, *Phys. Rev. B* **54**, 11169 (1996).
- [42] G. Kresse and J. Furthmüller, Efficiency of ab-initio total energy calculations for metals and semiconductors using a plane-wave basis set, *Comput. Mater. Sci.* **6**, 15 (1996).
- [43] J. Hutter, M. Iannuzzi, F. Schiffmann, and J. VandeVondele, CP2K: atomistic simulations of condensed matter systems, *Wiley Interdiscip. Rev.: Comput. Mol. Sci.* **4**, 15 (2014).
- [44] M. Guidon, F. Schiffmann, J. Hutter, and J. Van de Vondele, Ab initio molecular dynamics using hybrid density functionals, *J. Chem. Phys.* **128**, 214104 (2008).
- [45] D. Dexter, A theory of sensitized luminescence in solids, *J. Chem. Phys.* **21**, 836 (1953).
- [46] N. Itoh and M. Saidoh, Centres colores et impuretes radiation-induced dynamic motion of interstitial halogen in alkali halides, *J. Phys. (Paris) Colloq.* **34**, C9 (1973).
- [47] A. M. T. Allen, J. D. Comins, and P. J. Ford, Study of defect annealing in  $\gamma$ -irradiated KI by Raman scattering and optical absorption, *J. Phys. C: Solid State Phys.* **18**, 5783 (1985).
- [48] L. W. Hobbs, A. E. Hughes, D. Pooley, and P. B. Hirsch, A study of interstitial clusters in irradiated alkali halides using direct electron microscopy, *Proc. R. Soc. London. A. Math. Phys. Sci.* **332**, 167 (1973).